Int. J. Electron. Commun. (AEÜ) 135 (2021) 153728

Contents lists available at ScienceDirect

International Journal of Electronics and Communications

journal homepage: www.elsevier.com/locate/aeue

Regular paper

Digital pattern synthesis with a compact MIMO antenna of half-wavelength diameter

Abel Zandamela [a,b,c], Korbinian Schraml [c], Suramate Chalermwisutkul [b], Dirk Heberling [c,d], Adam Narbudowicz [a,e,*]

[a] CONNECT Centre, Trinity College Dublin, The University of Dublin, Dunlop Oriel House 34, Westland Row, Dublin 2, Ireland
[b] The Sirindhorn International Thai-German Graduate School of Engineering, King Mongkut's University of Technology North Bangkok, 1518 Pracharat 1 Rd. Wongsawang, Bangsue, Bangkok 10800, Thailand
[c] Institute of High Frequency Technology, RWTH Aachen University, Aachen 52074, Germany
[d] Fraunhofer Institute for High Frequency Physics and Radar Techniques FHR, Wachtberg 53343, Germany
[e] Department of Telecommunications and Teleinformatics, Wroclaw University of Science and Technology, Wroclaw 50-370, Poland

ARTICLE INFO

Keywords:
Pattern-reconfigurable antennas
Beamsteering
MIMO
Antennas for software defined radio
Compact antennas
Beamforming

ABSTRACT

The paper presents a compact multiport antenna, with beamforming capabilities and a realized gain of 4.31 dBi with the size of λ/2. The antenna allows digital beamforming with independent control over three parameters: main-beam direction, beamwidth, and null-depth. Those parameters can be dynamically adjusted within a continuous range, create multiple beams for different frequency channels, and simultaneously generate multiple digital patterns. Due to digital beamforming capabilities, the proposed antenna offers much greater flexibility over switch-based analogue beamforming of Electronically Steerable Parasitic Array Radiator (ESPAR) antennas. The reconfiguration properties are achieved by using superposition of three dipole-like radiation patterns, where each radiator generates different spherical mode, i.e. with different angular phase distribution in the horizontal plane. This allows beamsteering with compact size, while the use of different modes ensures low Envelope Correlation Coefficient (ECC) from 10^{-4} to 3.2×10^{-5} for the operating frequency of 2.4 GHz. The proposed technique allows for significantly greater pattern reconfiguration than any reconfigurable antenna or array of comparable size and is a perfect candidate for Software Defined Radios.

1. Introduction

Reconfigurable radiation pattern is a key requirement for many modern wireless systems, applicable to communication, radar and localization. It enables better spatial coverage, increased spectrum efficiency, improved link budget, and overall adaptability to changing propagation environment [1,2].

Conventional methods for pattern reconfiguration rely on using switching elements such as PIN diodes, MEMS, varactors, and others [1–17]. However, many of such structures have large electric dimensions. Among electrically-small reconfigurable antennas, in [3], a compact reconfigurable Huygens dipole is proposed, which switches between two unidirectional endfire patterns and a bi-directional one. In [4], a two-element array of size 0.62λ is reported to switch between conical and boresight patterns. Electronically Steerable Parasitic Array Radiator (ESPAR) antennas offer pattern reconfiguration by integrating one driven element surrounded by several parasitic ones [5–17]. Applying seven parasitic monopoles in [5] offers the gain of 4 dBi with 0.36λ aperture. Combining beam-switching and polarization reconfiguration with a microstrip antenna in [6] offers gains up to 3.5 dBi with significantly increased aperture of 1.2λ. Integrating orthogonally crossed dipoles in [7] offers a choice between 4 reconfigurable patterns with a reduced size of 0.42λ, however, the gain is reduced to 3.5 dBi. Using three printed monopoles was reported in [8] to allow increased gain of 6 dBi with aperture of 0.63λ. Other ESPAR compact designs also tend to use switches or tunable components [9–17], offering similar size/gain trade-offs. Even though ESPAR antennas exhibit many advantages, they are challenging for any frequency-division multiple access system, as they do not allow simultaneous use of multiple patterns across various frequency channels.

* Corresponding author.
E-mail addresses: zandamea@tcd.ie (A. Zandamela), schraml@ihf.rwth-aachen.de (K. Schraml), suramate.c.ce@tggs-bangkok.org (S. Chalermwisutkul), heberling@ihf.rwth-aachen.de (D. Heberling), narbudoa@tcd.ie (A. Narbudowicz).

https://doi.org/10.1016/j.aeue.2021.153728
Received 17 September 2020; Accepted 20 March 2021
Available online 27 March 2021

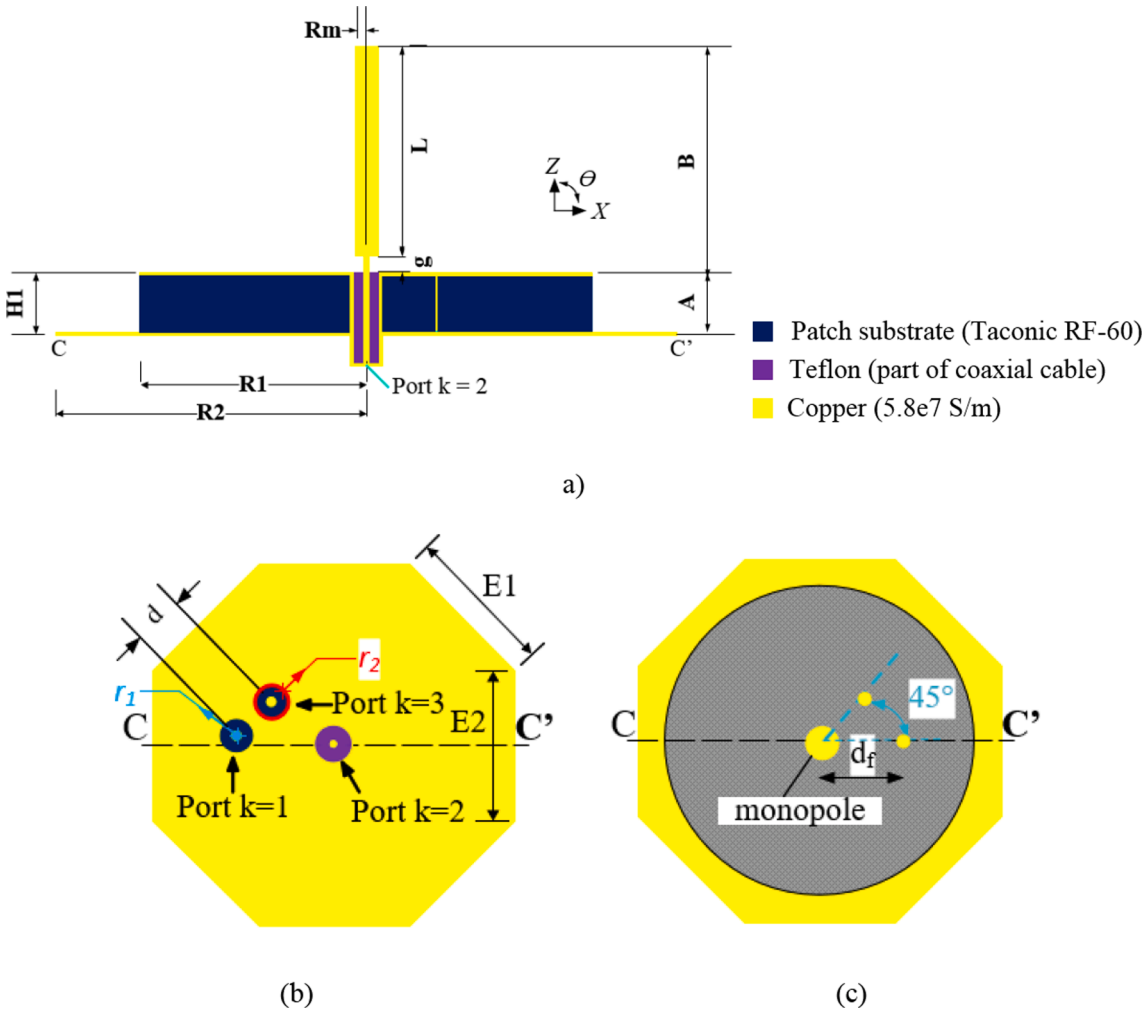

Fig. 1. Geometry of the proposed antenna. (a) Cut in *xz* – plane (vertical) following CC' dashed line. (b) Bottom view showing antenna groundplane and ports. (c) Top view showing pins arrangement on the circular patch.

The above disadvantage does not apply to antenna arrays and MIMO antennas, which can use techniques like digital beamforming to flexibly control the radiation patterns (e.g. adjust each frequency-channel independently or use multiple patterns simultaneously). However, classical antenna arrays are bulky structures, and there are few techniques that allow their miniaturization. A theoretical study presented in [18] shows the possibility to synthesize an extremely narrow beamwidth while using an antenna array of arbitrarily small size. However, such a super-directive radiation pattern is expected to have significantly reduced bandwidth [19].

MIMO antennas have the capability for flexible pattern reconfiguration using digital beamforming, while also supporting size reduction. By digitally adjusting amplitudes and phases of multiport antennas, multiple advantages have been reported. E.g.: two-dimensional beamsteering capabilities are investigated in [20]; null steering and limited beamsteering are proposed in [21]; three-dimensional null steering is discussed in [22,23]; adaptive null steering is demonstrated in [24]. In [25], a beam-reconfiguration around 360° is proposed using a dual-port antenna. However, all those solutions allow adjustment of only one parameter of the radiation pattern, be it either null steering or direction of the main beam.

This paper proposes a compact MIMO antenna for digital beamforming, with sufficient degrees of freedom to independently control three parameters: main beam direction, its beamwidth and null-depth. Unlike previous works, the proposed antenna allows to link parameters of the radiation pattern to specific parameters of antenna's excitation. This simplifies the calculation of desired radiation pattern and allows additional information about incoming signal, i.e. for angle of arrival applications. It should be also noticed, that in the proposed antenna all ports radiate into the same area, with the only distinction being the spatial phase distribution – a property desired for algorithms such as MUltiple SIgnal Classification (MUSIC). It allows realized gains of up to 4.31 dBi, while its diameter is only 0.5λ. The proposed technique offers superior flexibility over switch-based analogue beamsteering of ESPAR antennas, i.e. simultaneous generation of multiple patterns at the same frequency, or for different frequency channels. The design is easy to manufacture and offers low Envelope Correlation Coefficient (ECC) values from 10^{-4} to 3.2×10^{-5}, for the operating frequency of 2.4 GHz.

The remainder of this paper is organized as follows: Section 2 describes the antenna structure and parametric studies. Section 3 presents the measured results. Section 4 discusses how to control antenna's: main beam direction, beamwidth, and null-depth. Comparisons with ESPAR and antenna arrays are presented in Section 5; Conclusions are provided in Section 6.

2. Antenna design and simulation

2.1. Principle of operation

The principle for miniaturization can be best explained through spherical modes, which allow decomposition of 3D radiation pattern

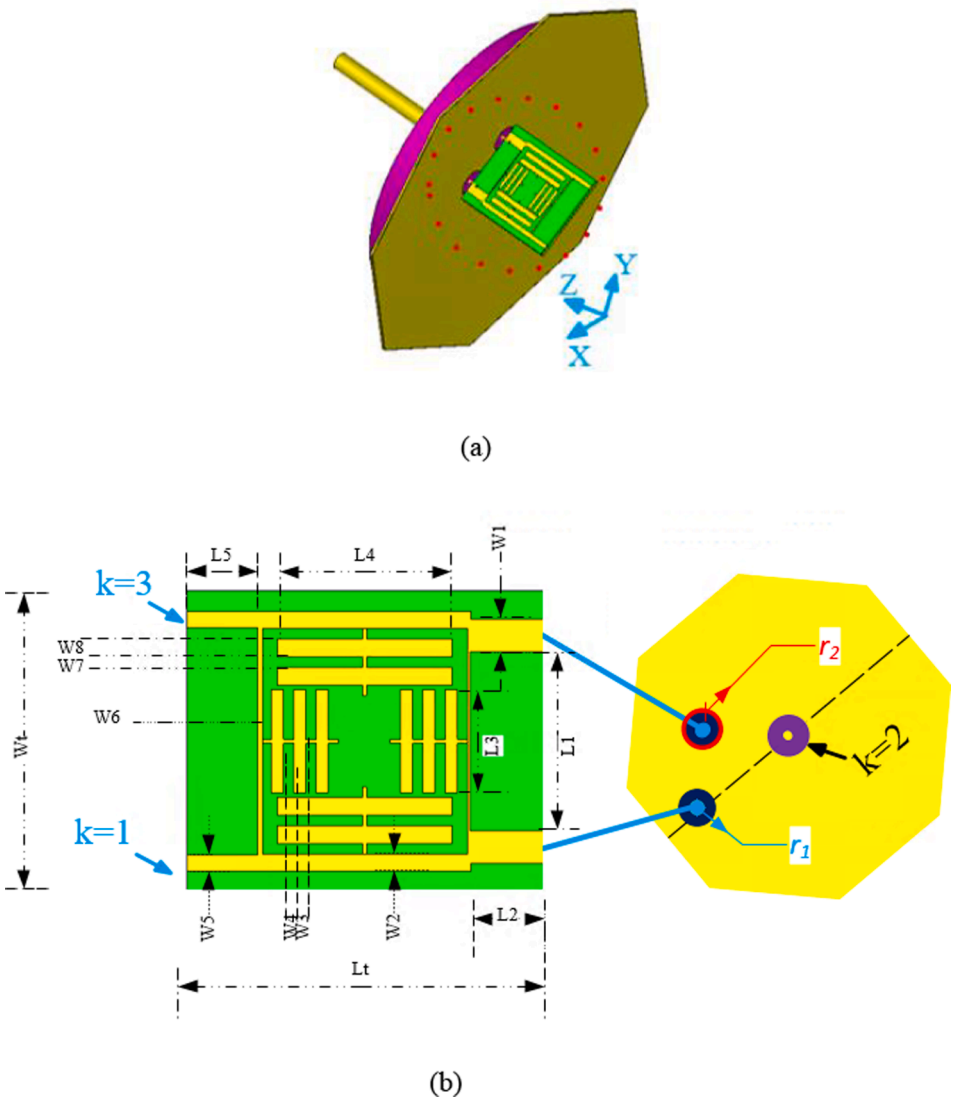

Fig. 2. Antenna and feeding system. (a) Perspective view of the proposed antenna with miniaturized coupler. The coupler is integrated vertically in respect to the octagonal groundplane, and its groundplane is connected with the antenna groundplane using a soldering layer. (b) Layout of the hybrid coupler, dimensions not drawn to scale; and schematic showing connections of hybrid coupler and circular patch feeding pins (shown in blue for visualization). (For interpretation of the references to colour in this figure legend, the reader is referred to the web version of this article.)

into a set of spherical modes [26]. Since – by definition – all modes are orthogonal to each other, they will result in a very low ECC [27]. The use of different modes offers an alternative approach to beamforming as demonstrated in [20–24,31,32]. However, unlike these works, we propose to use modes that exhibit same spatial amplitude distribution (omnidirectional), but with a linear progression of phase in the horizontal plane that can be described as:

$$ph_k(\phi) = 2\left(k - ceil\left(\frac{N}{2}\right)\right)\phi \tag{1}$$

where ϕ is an angle in the horizontal plane, k is the index of the port, N is the total number of ports used, and ceil is a ceiling rounding function. In the proposed antenna, N = 3. However more advanced designs utilising higher order modes and larger N are also feasible.

2.2. Antenna and feed system

The proposed antenna, implementing the above principle, is shown in Fig. 1. The circular disk is a higher-order resonant patch antenna, milled on a Taconic RF–60 substrate (relative permittivity $\varepsilon_r = 6$ and height $h = 6.35$ mm). The circular patch is designed to excite two orthogonal TM_{21} modes, i.e. each mode is excited independently through a pin soldered to the patch and a circular slot in the groundplane which is used to provide isolation between the vias and the groundplane (see Fig. 1b). The pin and the slot have radii of $r_1 = 0.25$ mm and $r_2 = 2$ mm, respectively. Since the patch resonates at higher-order modes, its principle of operation is different than in case of circularly polarized antennas: Two orthogonal TM_{21} modes have nodes oriented at 45° with respect to each other, with feeding pins located accordingly at a distance $d_f = 11.5$ mm from the patch centre (see Fig. 1c). These pins are intended to be excited simultaneously, through a hybrid coupler, with equal amplitude but ± 90° phase shift. Differently from classical patches, applying this principle results in a monopole-like radiation pattern, with the phase varying clockwise or counter-clockwise, depending on the sign of the phase shift. This implements in practice the principle proposed in (1) and will be denoted as port $k = 1$ for + 90° and $k = 3$ for −90° phase shift.

The monopole is represented by port $k = 2$ (see Fig. 1a). The structure protrudes above the top metallization of the patch, which serves as its groundplane. The base of the metallic rod of the monopole is located at $g = 2$ mm above the patch to achieve optimum 50 Ω match. The dimensions of the proposed antenna are (all in mm): $L = 28.5$, $E_1 = 26.16$, $E_2 = 27$, $R_m = 1.5$, $R_1 = 26.5$, $R_2 = 32$, $g = 2$, $H_1 = 6.35$, $r_1 = 0.25$, $r_2 = 2$, $d = 8.34$, and $d_f = 11.5$.

A miniaturized hybrid coupler is used as a feed circuit for ports $k = 1$ and $k = 3$. The miniaturization strategy is based on [28]. Its implementation is shown in Fig. 2. The coupler is realized on a low-cost FR-4

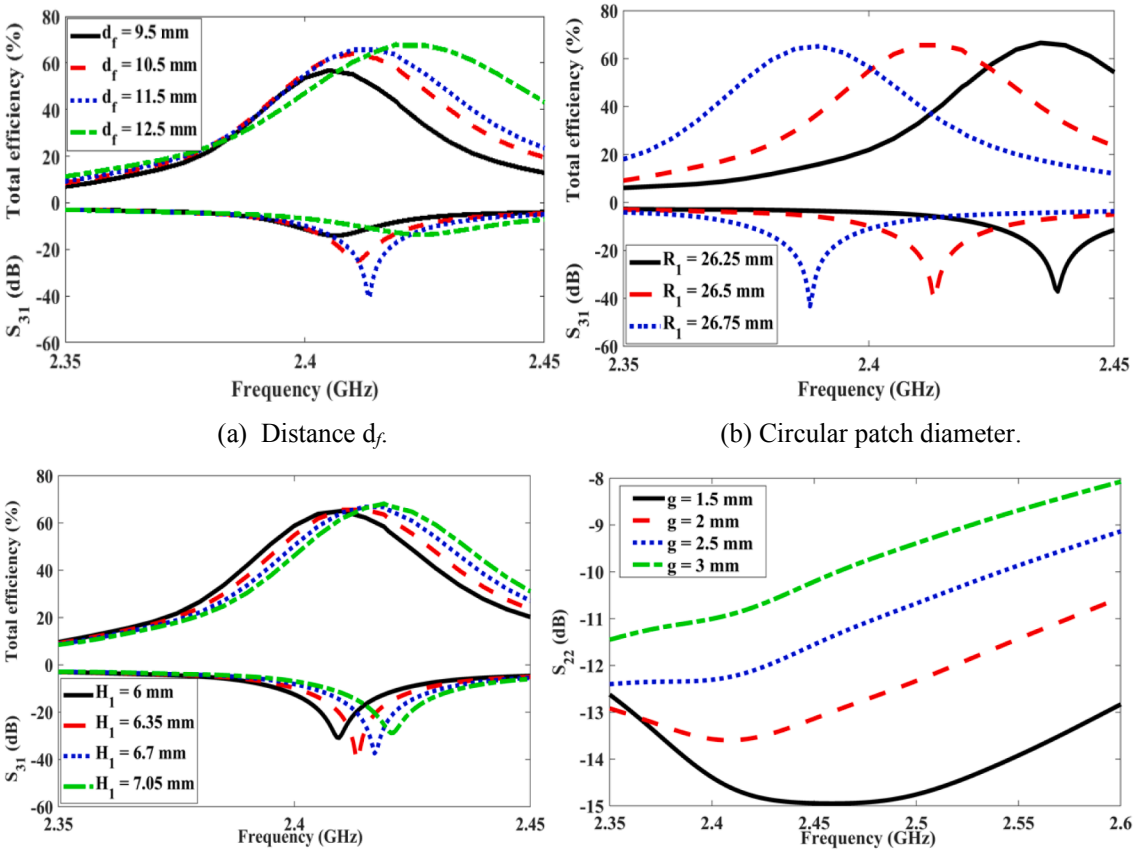

(a) Distance d_f. (b) Circular patch diameter.

(c) Thickness of the higher-order substrate. (d) Gap between patch and monopole.

Fig. 3. Isolation and total efficiency of the proposed antenna with different parameters.

substrate ($\varepsilon_r = 4.3$, $\tan\delta = 0.025$, height $h = 1$ mm). Two vias of radius $r_1 = 0.25$ mm connect the coupler to the antenna's circular patch (see Fig. 2b). Two circular holes of radius $r_2 = 2$ mm are milled into the octagonal groundplane around the vias. The dimensions of the coupler are (all in mm): $L_t = 17.5$, $W_t = 14.8$, $L_1 = 8.8$, $L_2 = 3.5$, $L_3 = 5.1$, $L_4 = 8.6$, $L_5 = 3.5$, $W_1 = 1.6$, $W_2 = 0.8$, $W_3 = 0.6$, $W_4 = 0.5$, $W_5 = 0.8$, $W_6 = 0.25$, $W_7 = 0.5$, $W_8 = 0.9$, $r_1 = 0.25$, and $r_2 = 2$.

2.3. Parametric studies

Parametric studies were conducted using full-wave electromagnetic simulations in CST Microwave Studio. Investigated parameters include the feeding pins distance d_f, the radius R_1 of the circular patch, the thickness H_1 of the substrate supporting the patch, and the gap g between the monopole and the patch. No significant difference between the total efficiency of ports $k = 1$ and $k = 3$ is observed, which is expected due to antenna's symmetry. Therefore, only the results of port $k = 1$ are presented.

Fig. 3a shows the isolation S_{31} between the ports $k = 1$ and $k = 3$, and the total efficiency of port $k = 1$ while changing parameter d_f. It can be seen that the center frequency shifts from 2.406 GHz to 2.424 GHz as d_f is increased from 9.5 mm to 12.5 mm. A slight increment in efficiency is observed when d_f is increased. The maximum isolation is at $d_f = 11.5$ mm, along with peak efficiency for the center frequency of 2.419 GHz. The simulation results depicted in Fig. 3b show that the radius R_1 impacts the center frequency. The frequency decreases from 2.439 to

(a) Top view (b) Bottom view (c)Vertical view (xz-plane)

Fig. 4. Photograph of the fabricated compact multiport reconfigurable antenna.

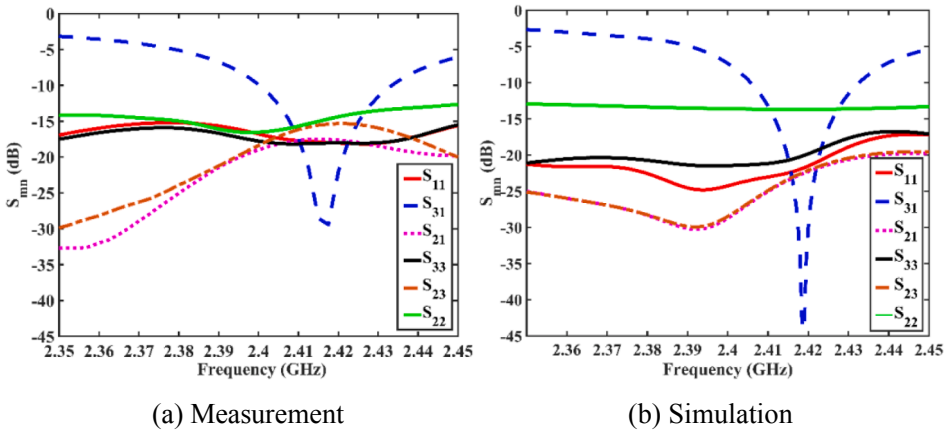

Fig. 5. Reflection and transmission coefficients of the proposed antenna.

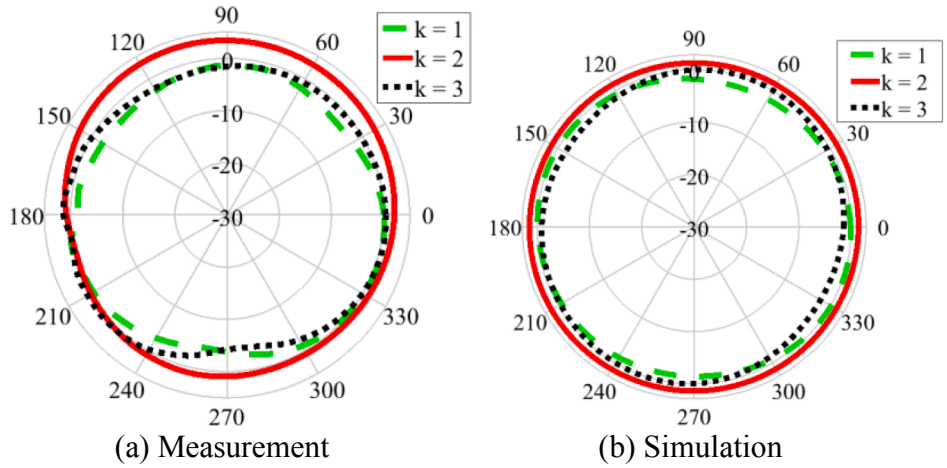

Fig. 6. Amplitudes of the proposed antenna at 2.4 GHz (vertical polarization) in xy − plane.

2.388 GHz, as the radius is increased from 26.25 mm to 26.75 mm. This is accompanied by an increase on the isolation from 37 to 43.2 dB. The impact on efficiency is negligible. The center frequency of 2.419 GHz is seen at $R_1 = 26.5$ mm.

The impact of the substrate thickness H_1 on the isolation and total efficiency is shown in Fig. 3c. The center frequency increases from 2.409 to 2.4205 GHz, and the efficiency slightly increases as H_1 is increased from 6 to 7.05 mm. The maximum isolation is seen at $H_1 = 6.35$ mm. It should be mentioned that the impedance bandwidth increases from 26.4 to 28.1 MHz as H_1 is increased. Fig. 3d shows the S-parameter results for port $k = 2$ when changing the gap g. It can be seen that the matching decreases as g is increased, and the center frequency shifts towards lower values. The center frequency of 2.419 GHz is seen at $g = 2$ mm.

The parametric results show that for better isolation characteristics of the proposed antenna, a good tuning of the feed location d_f is required. To control the center frequency, the patch radius R_1 should be varied. For bandwidth improvements, the substrate thickness H_1 should be increased. The matching of port $k = 2$ can be adjusted by using the gap g.

3. Fabrication and measurement

The antenna is prototyped as shown in Fig. 4. The monopole is directly fed using SMA connector. The patch is fed through a hybrid coupler, which is integrated vertically below the antenna's octagonal groundplane to minimize the impact on radiation properties.

The simulated and measured S-parameters are shown in Fig. 5a and 5b, respectively. The center operating frequency is 2.419 GHz, with a 34 MHz impedance bandwidth (2.401–2.435 GHz). This compares to the simulated bandwidth of 27 MHz (2.406–2.433 GHz) providing a good agreement. The antenna has a good isolation between all of its ports.

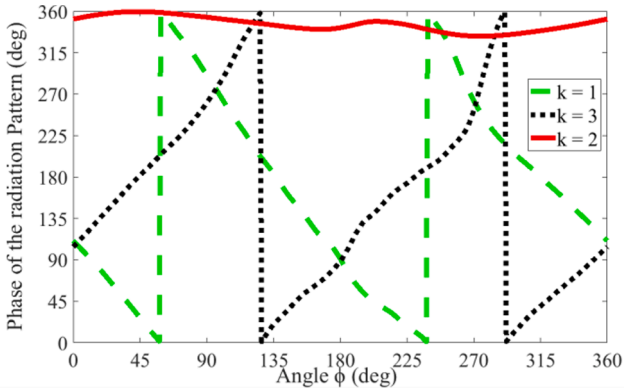

Fig. 7. Measured phase of the radiation pattern of the proposed antenna at 2.4 GHz (vertical polarization) in xy − plane.

Fig. 6a shows the measured radiation pattern at 2.4 GHz, in the horizontal plane (xy-plane in Fig. 1a) when each port is individually excited. The monopole ($k = 2$) exhibits slightly increased gain over the remaining ports, which is expected due to the lower efficiency of patch antennas, i.e. losses in the dielectric material.

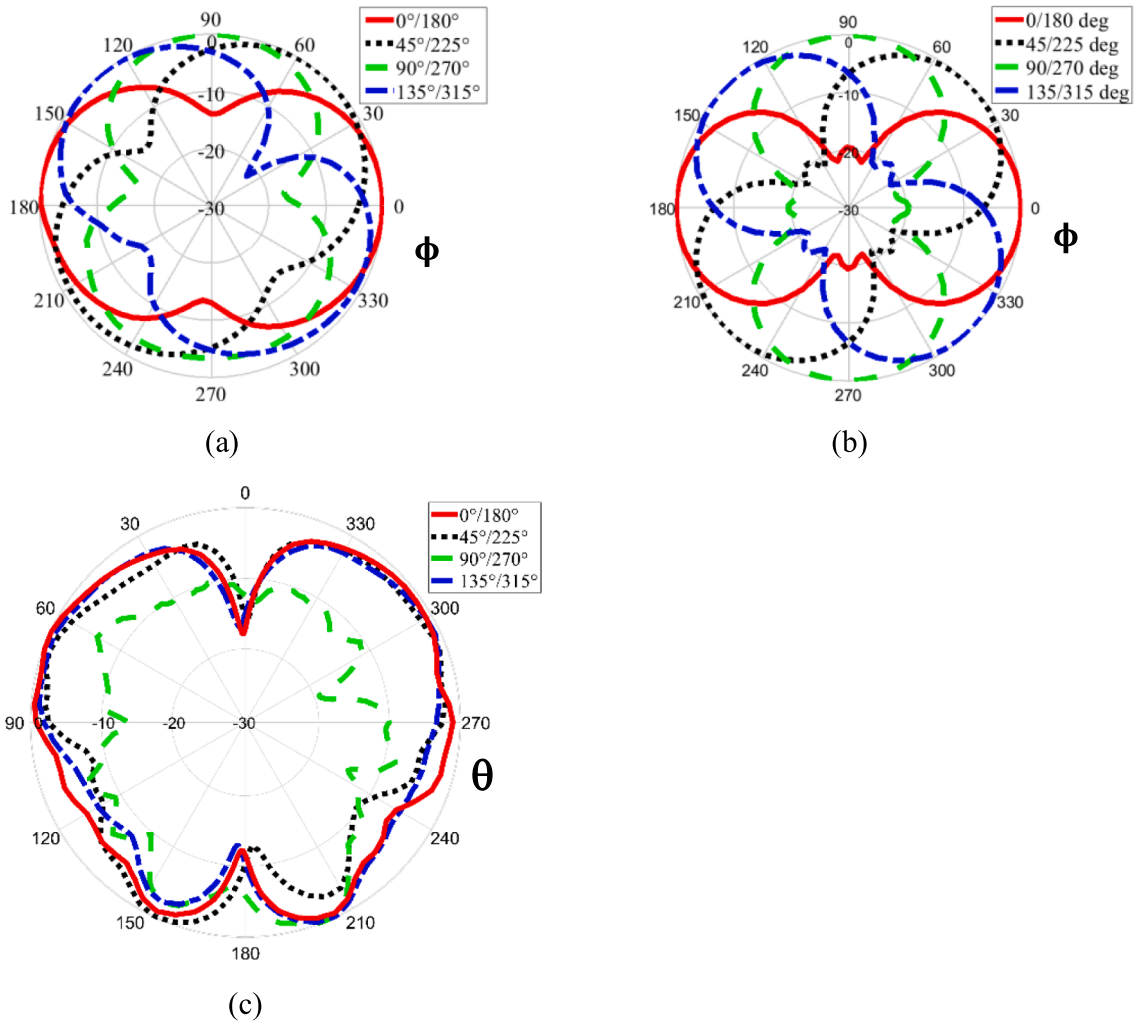

Fig. 8. Synthesized normalized radiation pattern (vertical polarization). (a) Measured patterns at 2.4 GHz in xy − plane. (b) Theoretical prediction obtained with (2). (c) Measured patterns at 2.4 GHz in xz − plane.

The phase of the radiation pattern for each port is depicted in Fig. 7. As expected, it follows the relation outlined in (1), albeit with the addition of a constant value that corresponds to different lengths of the feed cables. This property enables pattern synthesis despite the compact size of the antenna.

The ECC was calculated based on radiation patterns of each port [29] and is below 10^{-2} within antenna bandwidth. At 2.4 GHz the ECCs and the Multiplexing Efficiencies (ME) [36] are as follows between ports pairs *(1, 2):* ECC = 10^{-4}, ME = -1.29 dB; *(1, 3):* ECC = 5.5×10^{-5} and ME = -2.3 dB; *(2, 3)* ECC = 3.2×10^{-5} and ME = -1.29 dB. The simulated diversity gain (DG) [33], mean effective gain (MEG) [34] between all antenna ports are 9.99 dB and −3 dB, respectively. The total active reflection coefficient (TARC) [34] is −51.6 dB. The channel capacity loss (CCL) [35] is 0.38 bits/s/Hz. All above values are given for the center frequency 2.4 GHz.

Table 1
Applied phase shifts for the four investigated beam configurations.

Beam direction Φ_d	β_1	β_2	β_3
0°/180°	260°	0°	260°
45°/225°	350°	0°	170°
90°/270°	80°	0°	80°
135°/315°	170°	0°	350°

4. Radiation pattern synthesis

Based on (1), the synthesized radiation pattern in the horizontal plane *P(ϕ)* can be easily predicted using the simplified formula:

$$\mathrm{P}(\phi) = \frac{1}{\sqrt{N}} \sum_{k=1}^{N} w_k e^{j(2(k-2)\phi + C_k)} \tag{2}$$

where $w_k = a_k e^{j\beta_k}$ is a complex weighting factor applied at the k^{th} port; a_k and β_k are respectively the amplitude weighting and phase shift applied at the k^{th} port. Although real antenna will exhibit more nuanced properties, Eq. (2) allows good approximation for pattern synthesis with low computational complexity. This is demonstrated in subsequent sections.

4.1. Beam direction

Differently to antenna arrays, the proposed antenna's beam changes linearly with the applied phase shift. Without loss of generality, we will use port $k = 2$ as a reference with the constant phase. The phase shift required at two remaining ports to direct the beam into Φ_d can be calculated as:

$$\begin{aligned} \beta_1 &= 2 \times \Phi_d + C_2 - C_1 \\ \beta_3 &= -2 \times \Phi_d + C_2 - C_3 \end{aligned} \tag{3}$$

where C_k are constants representing phase addition due to cable length

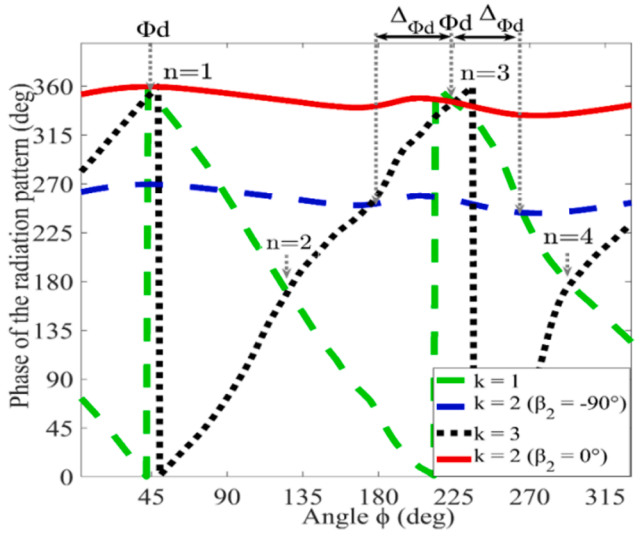

Fig. 9. Beamwidth broadening principle at 2.4 GHz (vertical polarization) in xy – plane for 45°/225° beam.

(here $C_1 = 110°$, $C_2 = -350°$, and $C_3 = 100°$).

Fig. 8 demonstrates four measured radiation patterns generated using (3) and separated by 45°. Fig. 8a shows the beamsteering in the horizontal plane (xy – plane). The corresponding phase shifts are shown in Table 1. The radiation patterns in xz – plane are shown in Fig. 8c. The shouldering visible in the pattern is due to the feeding cable perturbations. Nevertheless, the maximum of the pattern is located in xy – plane, and a null is visible at θ = 0°/180° directions. Fig. 8b shows the simplified radiation pattern calculated with (2) when using the same excitation coefficients. The gains for the measured cases are: 4.09, 4.31, 4.07, and 3.94 dBi, for the main beams directed respectively into 0°/180°, 45°/225°, 90°/270°, and 135°/315°. The corresponding 3 dB beamwidths are 83.8°, 85.8°, 73°, and 76.4°. This compares with 68°, 69°, 69°, and 69° beamwidths obtained with (2). This is because the simplified model assumes the same gain at each port. Nevertheless, the predictions may be used as an initial approximation.

4.2. Beamwidth

Synthesized beamwidth can be controlled by adding small perturbation to parameters β, as compared to the situation where all three ports interfere constructively at Φ_d ($n = 1, 3$ in Fig. 9). This is achieved by adjusting phase-shift at the reference port, here $k = 2$ (solid red line in Fig. 9). The main beam is then stretched, reducing the antenna's directivity by broadening

the beamwidth. However, the main beam direction remains the same at Φ_d.

Fig. 10a and 10b show the radiation patterns with varying beamwidths for the measured data and for the simplified model (2), respectively. It can be seen that as β_2 is perturbed, the beamwidth increases in all cases. The generated beam properties are summarized in Table 2.

It should be mentioned that as β_2 is further decreased (i.e. $\beta_2 < -70°$), the patterns become increasingly distorted up to the point of a pattern consisting of four beams. This is due to the antenna characteristics shown in Fig. 9, where it can be seen that in $n = 1, 2, 3, 4$ directions, ports 1 and 3 are in-phase (i.e. $ph_1(\phi) = ph_3(\phi)$), and for $\beta_2 = 0°$ the constructive interference directs the antenna main beams towards directions denoted as $n = 1, 3$. When β_2 is decreased but is still $\beta_2 > -70°$, the beam broadening condition: $\Phi_d \pm \Delta_\Phi$ is generated for the directions $n = 1, 3$. However, as $\beta_2 \approx -90°$, the broadening condition is also observed for other directions ($n = 2, 4$), resulting in a radiation pattern with four beams. For $\beta_2 = -90°$ the four main beams are seen at directions $\Phi_d + 90° \times n$ ($n = 0, 1, 2, 3$).

4.3. Null-depth

The magnitude of the input amplitudes a_k at each antenna port can be used to control the depth of the nulls of the radiation pattern. This is shown in Fig. 11 for the configuration $\Phi_d = 45°/225°$. It can be seen that for both cases, measured (Fig. 11a) and theoretical (Fig. 11b), the depth of the nulls decreases as the amplitude of the signal at port 1 decreases. This is accompanied by a slight decrease in the gain and increase of the beamwidth. Those changes are listed in Table 3 for the measured results. Comparable results were obtained by varying the amplitude of port 3 (with $a_2 = a_1$). If amplitudes of two ports are decreased simultaneously, the null-depth change doubles. The use of the antenna ports input amplitudes to control the depth of nulls can be combined with other

Table 2
Beam properties obtained from the 45°/225° configuration by controlling phase shift of port 2.

β_2	Beamwidth	Null-depth (dBi)	Gain (dBi)
0°	85.5°	−13.3	4.31
−30°	87.3°	−5.8	4.1
−60°	103.4°	−1.7	3.31
−70°	128°	−0.94	2.9

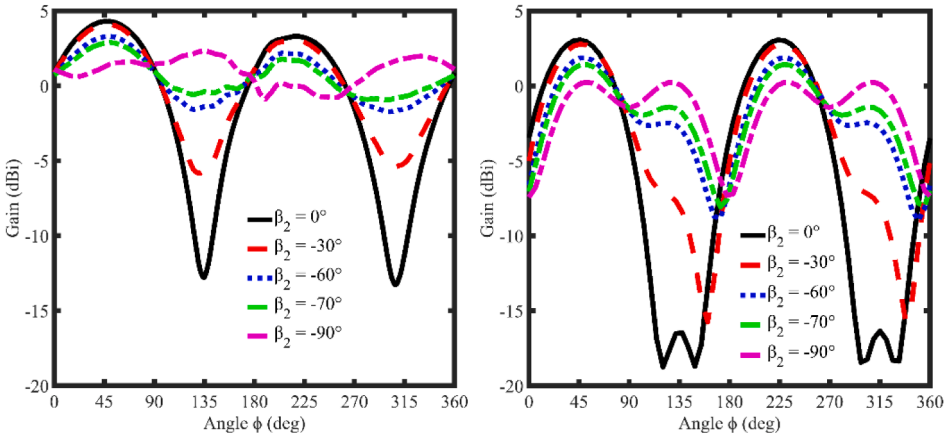

(a) Measured results. (b) Theoretical results from (2).

Fig. 10. Normalized synthesized radiation pattern (vertical polarization) in xy–plane, for the 45°/225° beam configuration using different phase shift values in port 2.

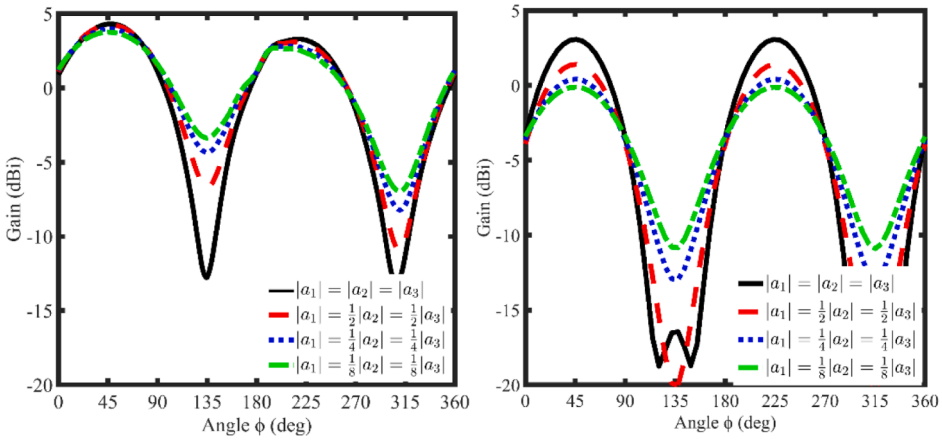

(a) Measured results. (b) Theoretical results from (2).

Fig. 11. Normalized synthesized radiation pattern (vertical polarization) in xy–plane, for the 45°/225° beam configuration using different amplitudes in port 1.

Table 3
Beam properties obtained from 45°/225° configuration by controlling amplitudes of port 1 ($a_2 = a_3$).

a_1	Beamwidth	Null-depth (dBi)	Gain (dBi)
a_2	85.5°	−13.3	4.31
1/2 a_2	90.4°	−10.9	4.25
1/4 a_2	96.3°	−8.2	3.98
1/8 a_2	101°	−7	3.8

discussed techniques, allowing flexible shaping of the radiation pattern.

5. Comparison with ESPAR-antennas and antenna arrays

A comparison of the proposed antenna with ESPAR antennas is detailed in Table 4. It is noted that contrary to the ESPAR antennas, where only a single port is used, the proposed antenna requires a total of 3 ports. This implies an increase of the RF modules, and the total energy needed by the system, a known disadvantage of MIMO systems. In terms of size and gain trade-off, the proposed antenna is comparable with ESPAR characteristics, offering 4.31 dBi from 0.5λ aperture. The two closest ESPAR antennas offer a slightly lower gain of 3.5 dBi at 0.42λ diameter [7] and a slightly higher gain of 6.05 dBi gain with a size of 0.63λ [8]. However, the main advantage of the proposed design is the digital beamforming capability, that is not achievable using ESPAR. Overall advantages of the proposed technique include a non-discrete configuration, faster adaptation time compared with a pattern configuration using externally controlled diodes, use of individualized beams for each frequency channel and the use of multiple radiation patterns at the same time.

The proposed multiport antenna is compared with 3-element linear and circular arrays in Table 5. The arrays have typical inter-element spacing of λ/2. The proposed antenna offer miniaturization by 35% to 66%, as compared to circular and linear arrays, respectively. Moreover,

Table 4
Comparisons of measured performance between the proposed antenna and ESPAR antennas.

Ref.	Size (λ × λ × λ)	Steering plane	Steering range (°)	Steering type	Multiple patterns	Number of ports	Beam-shaping	Gain (dBi)
[5]	0.36λ × 0.36λ × 0.33λ	Horizontal	D (0–360)	Discrete (N = 6)	No	1	No	4
[7]	0.42λ × 0.42 λ × 0.006λ*	Horizontal	D (0–360)	Discrete (N = 4)	No	1	No	3.5
This work	**0.5λ × 0.5λ × 0.3λ**	**Horizontal**	**B (0–360)**	**Continuous**	**Yes**	**3**	**Adjustable Beamwidth, Null-depth**	**4.31**
[8]	0.63λ × 0.59λ × 0.016λ	Horizontal	O & D	Discrete	No	1	No	6.05
[16]	0.63λ × 1.2λ × 0.2λ	Elevation	D (−26 to 20)	Continuous	No	1	No	5.5–6.1
[9]	0.8λ × 0.3λ × 0.01λ*	Elevation	D (−15 to 15)	Continuous	No	1	No	6.5–7.4
[12]	0.8 λ × 0.74λ × 0.1λ	Elevation, Horizontal	D	Discrete (N = 9)	No	1	No	~6.5
[11]	0.9λ × 0.9λ × 0.08λ	Elevation, Horizontal	D	Discrete (N = 6)	No	1	No	~5.18
[6]	1.2 λ × 1.2λ × 0.2λ	Horizontal	D,					
B (0–360)	Discrete (N = 10)	No	1	3 polarization states	2.5–3.5			
[15]	1.3λ × 1.3λ × 0.08λ*	Horizontal	D (0–360)	Discrete (N = 8)	No	1	No	7.3–7.5
[10]	1.44 λ × 1.44λ × 0.2λ	Horizontal	D	Discrete (N = 6)	No	1	No	10
[13]	1.5λ × 1.0λ × 0.58λ	Elevation	D (–32 to 32)	Discrete (N = 5)	No	1	No	8.5–9.3
[14]	1.58 λ × 1.58λ	Elevation	D (–22 to 22)	Continuous	No	1	No	6.6 ± 0.9
[17]	2.3 λ × 1.4λ × 0.06λ	Elevation	D (−27 to 29)	Continuous	No	1	No	5–5.2

D (Directional), O (Omnidirectional), and B (Bidirectional). * Indicates that the size of the groundplane is not specified, hence the total size of the antenna is larger than the values presented in the Table.

Table 5
Comparisons of measured performance between the proposed antenna and antenna arrays.

Antenna Type	Size (incl. groundplane)	Main beams	Number of ports	Beam direction (Φ_d)	3 dB Beamwidth	Gain (dB)
This Work	$0.5\lambda \times 0.5\lambda \times 0.3\lambda$	2 beams (always at 180°)	3	90°	73°	4.07
Linear array	$1.49\lambda \times 0.49\lambda \times 0.22\lambda$	2 beams mirroring each other	3	90°	37°	6.65
				32°	57.5°	4.84
Circular array	$0.76\lambda \times 0.76\lambda \times 0.22\lambda$	Single beam	3	90°	127°	4.76

the proposed antenna does not suffer from beam broadening that occurs in linear arrays when the beam is steered away from broadside directions. For the main beam directed at $\phi = 32°$ the linear array's beamwidth deteriorates to 57.5° (an increase of 20.5°), compared to a maximum beamwidth of 85.8° (maximum increase of 12.5°) for the proposed antenna at endfire $\phi = 0°$. For linear arrays the beamforming is limited to $0° - 180°$. The full horizontal plane can be obtained with circular array, however with increased beamwidth and larger overall size.

6. Conclusions

The paper proposes a MIMO antenna, with digital pattern synthesis comparable to switch-controlled ESPAR antennas. However, due to the use of multiport and digital beamforming, the proposed antenna offers functionality which cannot be realized with ESPAR, i.e. simultaneous generation of multiple beams or generation of different patterns for different frequency channels. The antenna offers 4.31 dBi of realized gain and is 0.5λ in diameter. Very low ECC between 10^{-4} to 3.2×10^{-5}, DG around 9.99 dB, TARC < -50 dB, CCL < 0.4 bits/s/Hz, allows its use for classical MIMO applications.

The paper also discusses how different parameters of the pattern can be adjusted including beam direction, beamwidth and null-depth. The structure can be further miniaturized by loading the circular patch substrate with a high-permittivity dielectric [30]. The proposed technique allows many advanced radio applications (e.g. angle of arrival, radar, MIMO) to be operated from a small platform.

Declaration of Competing Interest

The authors declare that they have no known competing financial interests or personal relationships that could have appeared to influence the work reported in this paper.

Acknowledgments

This work was partially supported by the German Academic Exchange Service (DAAD) under the Master's scholarship with the student mobility grant to RWTH Aachen University, by King Mongkut's University of Technology North Bangkok, Contract no. KMUTNB-BasicR-64-30, and in part by Science Foundation Ireland, grants no. 18/SIRG/5612 and 13/RC/2077. The authors thank A. Polaczek and C. L. Cullota from RWTH Aachen University for their help with the antenna measurement and R. Wirtz and O. Nicolae for their help in prototyping.

References

[1] Boerman JD, Bernhard JT. Performance study of pattern reconfigurable antennas in MIMO communication systems. IEEE Trans. Antennas Propag. 2008;56(1):231–6.
[2] Costantine J, Tawk Y, Barbin SE, Christodoulou CG. Reconfigurable antennas: design and applications. Proc. IEEE 2015;103(3):424–37.
[3] Wu Z, Tang M-C, Li M, Ziolkowski RW. Ultralow-profile, electrically small, pattern-reconfigurable metamaterial-inspired huygens dipole antenna. IEEE Trans Antennas Propag 2020;68(3):1238–48.
[4] Li H, Lau BK, He S. Design of closely packed pattern reconfigurable antenna array for MIMO terminals. IEEE Trans. Antennas Propag. 2017;65(9):4891–6.
[5] Liu H-T, Gao S, Loh T-H. Electrically small and low cost smart antenna for wireless communication. IEEE Trans Antennas Propag 2012;60(3):1540–9.
[6] Gu C, Gao S, Liu H, Luo Q, Loh T-H, Sobhy M, Li J, Wei G, Xu J, Qin F, Sanz-Izquierdo B, Abd-Alhameed RA. Compact smart antenna with electronic beam-switching and reconfigurable polarizations. IEEE Trans Antennas Propag 2015;63(12):5325–33.
[7] Zhang L, Gao S, Luo Q, Young PR, Li Q. Planar ultrathin small beam-switching antenna. IEEE Trans. Antennas Propag. 2016;64(12):5054–63.
[8] Marantis L, Rongas D, Paraskevopoulos A, Oikonomopoulos-Zachos C, Kanatas A. Pattern reconfigurable ESPAR antenna for vehicle-to-vehicle communications. IET Microw Antennas Propag. 2018;12(2):280–6.
[9] Luther JJ, Ebadi S, Gong X. A microstrip patch electronically steerable parasitic array radiator (ESPAR) antenna with reactance-tuned coupling and maintained resonance. IEEE Trans. Antennas Propag. 2012;60(4):1803–13.
[10] Liu H, Gao S, Loh T-H. Small director array for low-profile smart antennas achieving higher gain. IEEE Trans. Antennas Propag. 2013;61(1):162–8.
[11] Nikkhah MR, Loghmannia P, Rashed-Mohassel J, Kishk AA. Theory of ESPAR design with their implementation in large arrays. IEEE Trans. Antennas Propag. 2014;62(6):3359–64.
[12] Li Z, Ahmed E, Eltawil AM, Cetiner BA. A beam-steering reconfigurable antenna for WLAN applications. IEEE Trans. Antennas Propag. 2015;63(1):24–32.
[13] Shahadan NH, Jamaluddin MH, Kamarudin MR, Yamada Y, Khalily M, Jusoh M, et al. Steerable higher order mode dielectric resonator antenna with parasitic elements for 5G applications. IEEE Access 2017;5:22234–43.
[14] Movahedinia R, Sebak A-R, Chaharmir MR, Nikkhah MR, Kishk AA. X-band circularly polarized electronically steerable parasitic array radiator of DRA. IEEE Trans. Antennas Propag. 2018;66(2):721–8.
[15] Burtowy M, Rzymowski M, Kulas L. Low-Profile ESPAR antenna for RSS-based DoA estimation in IoT applications. IEEE Access 2019;7:17403–11.
[16] Ouyang W, Gong X. An electronically steerable parasitic array radiator (ESPAR) using cavity-backed slot antennas. IEEE Antennas Wirel. Propag. Lett. 2019;18(4):757–61.
[17] Shu J, Xu G, Peng H, Mao J. An electrically steerable parasitic array radiator in package based on liquid crystal. IEEE Antennas Wirel. Propag. Lett 2019;18(11):2365–9.
[18] Arslanagić S, Ziolkowski RW. Highly subwavelength, superdirective cylindrical nanoantenna. Phys. Rev. Lett. 2018;120:6.
[19] Hansen RC. Electrically Small, Superdirective, and Superconducting Antennas. John Wiley & Sons; 2006.
[20] Labadie NR, Sharma SK, Rebeiz GM. Investigations on the use of multiple unique radiating modes for 2-D beam steering. IEEE Trans. Antennas Propag. 2016;64(11):4659–70.
[21] Babakhani B, Sharma SK. Dual null steering and limited beam peak steering using triple-mode circular microstrip patch antenna. IEEE Trans. Antennas Propag. 2017;65(8):3838–48.
[22] Deng C, Li Y, Zhang Z, Feng Z. A hemispherical 3-D null steering antenna for circular polarization. IEEE Antennas Wirel. Propag. Lett. 2015;14:803–6.
[23] Dicandia FA, Genovesi S, Monorchio A. Advantageous exploitation of characteristic modes analysis for the design of 3-D null-scanning antennas. IEEE Trans. Antennas Propag. 2017;65(8):3924–34.
[24] Iqbal Z, Pour M. Amplitude control null steering in a multi-mode patch antenna. Prog. Electromag. Res. Lett. 2019;82:107–12.
[25] Narbudowicz A, Ammann MJ, Heberling D. Switchless reconfigurable antenna with 360° steering. IEEE Antennas Wirel. Propag. Lett. 2016;15:1689–92.
[26] Hansen JE. Spherical Near-field Antenna Measurements. London, U.K: P. Peregrinus on behalf of the Institution of Electrical Engineers; 1988.
[27] R. Cornelius, A. Narbudowicz, M.J. Ammann, D. Heberling, Calculating the envelope correlation coefficient directly from spherical modes spectrum, in: 2017 11th European Conference on Antennas and Propagation (EUCAP), 2017.
[28] Liao S-S, Peng J-T. Compact planar microstrip branch-line couplers using the quasi-lumped elements approach with nonsymmetrical and symmetrical T-shaped structure. IEEE Trans. Microw Theory Tech. 2006;54(9):3508–14.
[29] Sharawi MS. Current misuses and future prospects for printed multiple-input, multiple-output antenna systems [Wireless Corner]. IEEE Antennas Propag. Magaz. 2017;59(4):162–70.
[30] A.A. Zandamela, K. Schraml, V. Jantarachote, S. Chalermwisutkul, D. Heberling, M.J. Ammann, A. Narbudowicz, On the efficiency of miniaturized 360° beam-scanning antenna, in: 2019 13th European Conference on Antennas and Propagation (EuCAP), 2019.
[31] L. Shafai, Scan gain enhancement in phased arrays by element pattern synthesis, in: Proc. IEE 7th Int. Conf. Antennas Propag. (ICAP), Apr. 15–18, 1991, vol. 2, pp. 914–917.
[32] Johannsen NL, Hoeher PA. Single-element beamforming using multi-mode antenna patterns. IEEE Wirel. Comm. Lett. 2020;9(7):1120–3.
[33] Kildal P, Rosengren K. Correlation and capacity of MIMO systems and mutual coupling, radiation efficiency, and diversity gain of their antennas: simulations and

measurements in a reverberation chamber. IEEE Comm. Magaz. 2004;42(12):104–12.
[34] Glazunov AA, Molisch AF, Tufvesson F. Mean effective gain of antennas in a wireless channel. IET Microw Antennas Propag. 2009;3:101–14.
[35] Chae SH, Oh S, Park S. Analysis of mutual coupling, correlations, and TARC in WiBro MIMO array antenna. IEEE Antennas Wirel. Propag. Lett. 2007;6:122–5.
[36] Tian R, Lau BK, Ying Z. Multiplexing efficiency of MIMO antennas. IEEE Antennas Wirel. Propag. Lett. 2011;10:183–6.